

Investigating the Impact of Waterhead, Time and Temperature on Dam Displacement: Application of Computer Aided Models

Maaz Abdullah

Follow this and additional works at: <https://ates.alayen.edu.iq/home>



Part of the [Engineering Commons](#)



ORIGINAL STUDY

Investigating the Impact of Waterhead, Time and Temperature on Dam Displacement: Application of Computer Aided Models

Maaz Abdullah

Civil and Environmental Engineering Department, King Fahd University of Petroleum & Minerals, Dhahran 31261, Saudi Arabia

ABSTRACT

Dam displacement is a crucial indicator for assessing the safety of a concrete dam through structural health monitoring. Since the displacement data exhibits a non-linear and complex relationship with influencing factors like waterhead, time and temperature, machine learning models are deployed to accurately predict dam displacement. Furthermore, the limited availability of monitored data in the majority of the dams renders the studies conducted with a large number of observations valueless. In order to address the aforementioned issues, this study proposes a feature selection approach to predict dam displacement by examining the ability of four ensemble machine learning models on different input combinations. The results reveal that the extreme gradient boost performs the best with a coefficient of determination (R^2) and RMSE value of 0.960 and 0.275 mm respectively. Random forests and decision tree models exhibited better performance on using single predictor variables waterhead and age respectively. AdaBoost exhibited moderate performance but was unaffected by the negative influence of extra predictor variables. The comparison results indicated that models developed with only ambient air temperature as input data are insufficient to predict dam deformation. The outcomes of this study are resourceful in prioritizing models based on the data availability for accurate prediction of dam displacement.

Keywords: Dam displacement, Concrete dam, Machine learning, Feature selection, Random forests

1. Introduction

Dams are structures built across the flow of water to serve multiple purposes. In addition to being the foundation for maximizing the temporal-spatial distribution of water resources, dam safety has a significant impact on biological ecosystems and social development [1, 2]. Their role in mitigating the effects of floods and droughts has inspired several nations to consider them an asset to their economy. They also support the socio-economic growth of a country by facilitating flood control, hydropower generation, and off-season water storage for irrigation purposes, as well as recreational activities and tourism [3]. Floods and landslides prone regions have benefited intensively from the presence of dams built

upstream to their community as they could issue warnings earlier [4]. Concrete gravity dams are one of the most commonly built structures for retaining water in wide river valleys and often rise over 70 m [5, 6]. They are deemed to be more adaptive to topographical and geographical conditions of an area and generally utilize their self-weight to maintain stability from upstream hydraulic pressure and other miscellaneous loads [7].

The functioning of a concrete dam is connected with complex inherent mechanical qualities and the consideration of a diversity of external loads [8]. The safety of dams can be jeopardized by a variety of risk factors and is eventually deemed as a significant social issue. These variables cover a broad diversity of effects, such as excessive external stresses,

Received 20 March 2025; revised 5 April 2025; accepted 9 April 2025.
Available online 30 April 2025

E-mail address: maazabdullah.alig@gmail.com (M. Abdullah).

<https://doi.org/10.70645/3078-3437.1028>

3078-3437/© 2025 Al-Ayen Iraqi University. This is an open-access article under the CC BY-NC-ND license (<https://creativecommons.org/licenses/by-nc-nd/4.0/>).

poor design and construction, aging materials, and increased human activity around dams [9, 10]. The combination of these elements highlights the intricate interactions that endanger the stability of dams and is responsible for drawing further public attention to the problem in recent years. It is also deemed essential to keep up with the evaluation of monitoring data of dams to understand the potentially deteriorating influence of external parameters like weather and climate, surroundings and aging impacts. The predicted changes in precipitation patterns driven by climate change, in addition to the increased frequency and intensity of extreme weather events, would probably cause dam failure that exceeds present design parameters [11, 12]. For the purpose of ensuring the safe operation of the dam, it is equipped with several monitoring sensors at various points to track structural reactions such as displacement, seepage, tension, and strain. Among the aforementioned reactions, the track record of dam displacement is easily accessible and is a fairly straightforward indicator of overall dam performance [13].

Owing to the factual information about the low adaptability of concrete dams for deformation, displacements can often be visualized on the application of external loads and subsequently considered as a key index for determining dam safety [14]. Failure seldom happens due to the degradation of dam material with time or through the application of the sudden increase in external loads [15]. Conversely, concrete gravity dams are known to resist sudden failures, and their deformation can be easily observed through long-term monitoring of dam behavior. This also provides the potential opportunity to develop feasible solutions [16]. In order to track performance indicators like deformation, cracking, stress, and strain, various monitoring equipment, including plumb lines, strain gauges, osmometers, and thermometers, are placed in strategic locations within the dam body of contemporary concrete dams [17]. Recent years have witnessed an increment in data availability by automatizing monitoring devices. Scholars [18] instigated the requirement of precise estimation of the deformation field to ensure a dam's serviceability and safe operation.

A frequently used approach for estimating dam deformation is numerical models based on the finite element method (FEM). These models ground their simulation results on the physical principles controlling the behavior of the operation [19]. FEM simulation, which is useful to analyze the operation safety status of dams, can generate the dam deformation field based on the parameter inversion approach [20, 21]. Another approach deployed by [22] is to estimate the hydrostatic component of dam displace-

ments by introducing spatial coordinates and utilizing FEM. He then built a three-dimensional hybrid model for a concrete arch dam. However, some measures of dam safety highlight the limitations of numerical models [23, 24].

The literature presented several empirical formulations to simulate dam displacement that are dependent on several constant coefficients and physical or climate parameters. However, those empirical equations were established in a particular case study and require certain assumptions for their conceptualization and thus, it is difficult to give the general expression for their utility. In addition, those formulations need a huge dataset for their development. For the foregoing reasons, the development of new technologies on dam displacement prediction is highly urged. Future predictions can be achieved through data-driven models that are built by the analysis of historical monitoring data of dam deformation. When the anticipated deformation value in the model differs from the actual measured deformation value by more than the specified warning thresholds or safety margins, an early warning can be generated [19, 25]. The displacement of a concrete dam is a crucial time-varying deformation performance indicator. It typically exhibits a complex nonlinear relationship with internal and external influencing factors, including water and air temperatures, the aging effects of concrete, hydrostatic pressure, and other unobserved factors [26]. The statistical models and machine learning models are the two primarily used data-driven models. Statistical models are well-known for their straightforward principles and ease of use. They are a vital tool for analyzing and inferring the distribution law and trend of data [24]. Over the course of its lengthy history, the statistical modeling known as the Hydrostatic-Season-Time (HST) model has produced well-established theories and found effective applications in real-world engineering [27, 28]. By altering the seasonal function using methods such as double support vector regression, periodic harmonic components, Gaussian process regression, and others, researchers have recently attempted to improve the accuracy of the HST model in representing the thermal deformation effects of concrete dams [13, 29]. However, it has been noted that HST encounters problems in handling extensive monitoring data [30].

In recent times, the use of soft computing models has widely increased in the field of hydraulics and hydrology [28, 31]. The advancement in the development of machine learning methods for data-based predictive modeling has replaced conventional statistical tools [32]. The limitations of the conventional statistical method may be overcome by the extensively used machine learning techniques in

the structural health monitoring of dams [33, 34]. An inherent advantage of displacement prediction models created using machine learning techniques is their ability to handle large amounts of multidimensional nonlinear data [35]. Multiple advanced ML models including support vector machines [36], artificial neural networks [37], convolution neural networks [38], random forests [39], Gaussian process regression [40], long-short term memory model [41], and adaptive neuro fuzzy inference systems [42] have been deemed as novel models for prediction of dam displacement and deformation. The use of ensemble models with decision trees as a foundational learner is becoming more and more popular due to their simplicity and ease of interpretation [43, 44]. Numerous researchers have deployed ensemble models like gradient-boosting decision trees (GBDT) [45], random forest (RF) [39, 46], extreme gradient boosting (XGB) [47], adaboosting (ADB) [48], and light gradient boosting machine (LGBM) [49] for similar studies. Various researchers have also emphasized that ensemble models produce acceptable results on limited data availability and are more reliable for getting better performance [50–52].

To tackle the problem of limited data availability and remove the dependency of continuous data monitoring for time series analysis, this study proposes a comparison of modern-day ensemble machine learning models based on a decision tree for dam displacement prediction. These multiple regression models decompose the displacement observed into three components, namely, hydrostatic, aging and temperature. A feature selection approach is integrated to analyze the dependency of displacement based on different subsets of independent variables. To effectively evaluate the performance of considered machine learning models, multiple performance indices are deployed.

2. Methodology overview

2.1. Decision trees (DT)

A supervised learning model that maps a data domain hierarchically onto a response set is called a decision tree. A data domain (node) is split recursively into two subdomains so that the information gain of the subdomains is greater than that of the split node. Since data categorization is the known objective of supervised learning, information gain is the degree to which the split's produced subdomains are easily classified. The optimization algorithm in decision tree-based supervised learning seeks to identify the optimal split that maximizes information gain or the ease of categorization [53]. The nodes used in

decision trees come in three variations: root nodes, internal nodes and leaf nodes.

DTs are stimulated by algorithms that create decision nodes based on predetermined cases. Using a fitness function minimization approach, the implemented algorithm seeks to identify the best DT. Regression models are fitted to the target variable using each of the independent variables because the dataset used in this article does not contain classes. Each independent variable has its dataset divided at many split points. The implemented algorithm determines the difference between the actual and expected values concerning the pre-established fitness function at each split point. The variable generating the lowest fitness function value is selected as the split point after a comparison of the split point errors for each variable.

For the prediction of dam displacement, the set of predictor variables $X = \{X_1, X_2, X_3\}$ contains water-head, age of dam, and temperature. Fig. 1 describes how the nodes of decision trees split the data involved for accurate prediction of displacement.

2.2. Extreme gradient boosted (XGB)

The eXtreme Gradient Boosting package, or XGBoost for short, is made to be effective, adaptable, and portable. An effective tree learning method and a linear model solver are included in the package. It is compatible with multiple objective functions, including regression, classification, and ranking. This gradient-boosting framework optimization and implementation is scalable, effective, and efficient [54]. By controlling the model's complexity, a regularized model prevents overfitting and simplifies the learning model. When choosing the optimal dividing points for enumeration, it uses parallelization, which accelerates training. When the forecast is accurate, the tree building is halted early on, accelerating the training pace [55].

Gradient boosting works on the fundamental principle that a group of weak learners will provide a better score than any single weak learner. The gradient boosting framework is normally expressed as:

$$F^m(x) = \sum_{i=1}^m \beta_i t_i(x) \quad (1)$$

Where m is the number of weak learners involved in the development of the algorithm, t is the weak learner and β is the coefficient.

By building a set of functions $F^0, F^1, F^2, \dots, F^m, \dots, F^n$ and a certain learning rate (α), the gradient-boosted decision trees train iteratively. The loss function

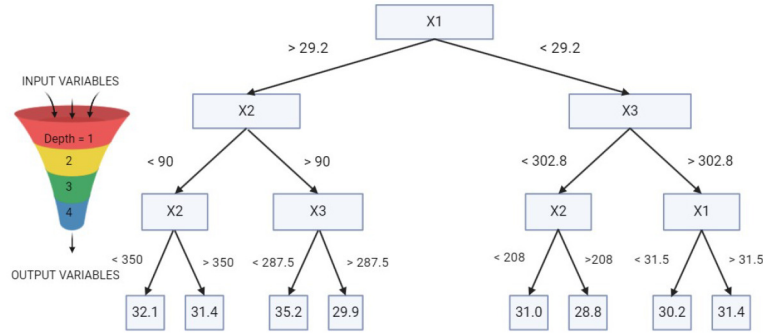


Fig. 1. An exemplary decision tree that can be created for dam displacement prediction.

$L(y_i, F_m)$ can be improved by identifying another function, $F_{k+1} = F_k + t_{k+1}(X)$, such that t_{k+1} minimizes the anticipated value of the loss function. Take into consideration the output values $\{y_1, y_2, y_3 \dots y_m\}$ corresponding to the set of predictor variables $\{X_1, X_2, X_3 \dots X_m\}$. For each t , the set of Decision Trees that should be added to the ensemble is the contender.

$$t^{m+1} = \operatorname{argmin} L(y, F^m) \tag{2}$$

Therefore, the next function F^{m+1} is generated as follows:

$$L(y, F^{m+1}) = L(y, F^m + t^{m+1}) \tag{3}$$

The XGBoost algorithm further involves a convex function and the term ‘ Ω ’ for integrating the complexity of all the regression trees involved in the model.

2.3. Random forests (RF)

Random forest (RF) was originally introduced by [56] as an extended version of the DT predictor. The utilization of RF for application in water resource management with emphasis on dams has been depicted by various research [57, 58]. In recent years, the RF algorithm has been considered an extraordinarily strict learning algorithm despite its bias for high-level variables among categorical variables with different levels. The first step in the RF algorithm’s operation is the random sample collection from the given data. In the second step, a DT will be built for every sample. The final forecast produced by RF is the result of merging the predictions from several decision trees.

The average or total of all predictions is the result of training each tree using a different subset of the training data. The average of the forecasts from individual decision trees yields the final prediction. It is possible to manually adjust a number of parameters

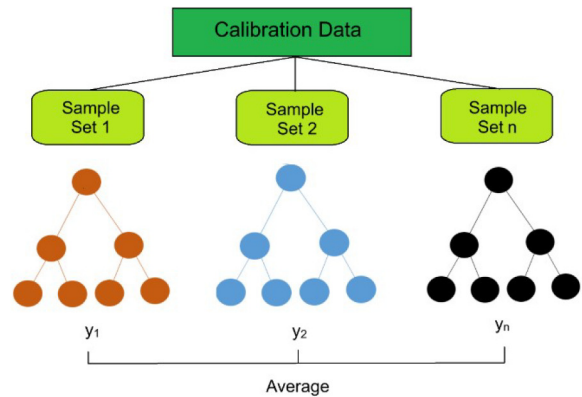


Fig. 2. Working of a random forest model.

for better outcomes, including the number of estimators, the maximum depth of the tree, the minimum number of samples needed for splitting nodes, the minimum number of leaves, the weight of the leaves, and whether to bootstrap at every tree or start a warm start.

For a set of output variables $\{y_1, y_2, y_3, \dots, y_n\}$ from n number of DT, the RF prediction will be given as follows:

$$y_{rf} = \frac{1}{n} \sum_{i=1}^n y_i \tag{4}$$

A basic schematic diagram of the working model of RF can be seen in Fig. 2.

2.4. AdaBoost regression (ADB)

AdaBoost algorithm, or adaptive boosting, is an ensemble model and works on the principle of improving the accuracy of weak learners by altering the weight distribution. It is one of the most used algorithms in integrated learning due to its capability of combining with other frameworks [48]. This

algorithm was initially introduced by [59] to adapt against the regression accuracies. The AdaBoost regressor creates weak regressors with high bias error but low variance error by continuously reweighting training examples depending on the prediction error with each boosting iteration. In doing so, the subsequent regressor highlights instances in which the initial phase's predictions proved to be incorrect. The final prediction is generated by summing the results of each weak regressor, which results in a model with fewer bias errors and low variance [60, 61].

Consider the training set $\{X_i, y_i\}_{i=1}^n$, the output regression can be denoted by $F(x)$, and the weight of the sample can be written as W_t , where $t = 1, 2, 3, \dots, n$ are used for training purposes. The maximum error generated after t iterations for basic learner $F_t(x)$ is calculated as below:

$$E_t = \max |y_i - F_t(x_i)| \quad (5)$$

For the i^{th} sample, the relative error is calculated according to the linear error method:

$$e_{ti} = 1 - e^{-\frac{|y_i - \hat{r}_i(x_i)|}{E_t^2}} \quad (6)$$

The weight coefficient α_t of the proportion of the t -th base learner $F_t(x)$ in the final strong learner is found based on the computed regression error rate ε_t . Following an iteration, the sample error is used to update the weight value of $F_t(x)$. Following the $t+1$ iteration, the W_{t+1} expression is:

$$W_{t+1} = (\omega_{t+1,1}, \omega_{t+1,2}, \omega_{t+1,3} \dots \omega_{t+1,n}) \quad (7)$$

$$\omega_{t+1,i} = \frac{\omega_{ti}}{Z_i} \alpha_t^{1-e_{ti}} \quad (8)$$

where Z is the Z-score normalization factor, such that the sum of weights is limited to 1.

The final stronger learner $F^n(x)$ can be described as:

$$F^n(x) = \sum_{i=1}^T \ln\left(\frac{1}{\alpha_t}\right) f(x) \quad (9)$$

Where $f(x)$ is the mean of $\alpha_t * F_t(x)$ for all the iterations $t = 1, 2, 3 \dots n$.

2.5. Modeling development procedure

The ability of the ensemble ML models to accurately predict dam displacement is examined by deploying four algorithms, namely, DT, XGB, RF and ADB.

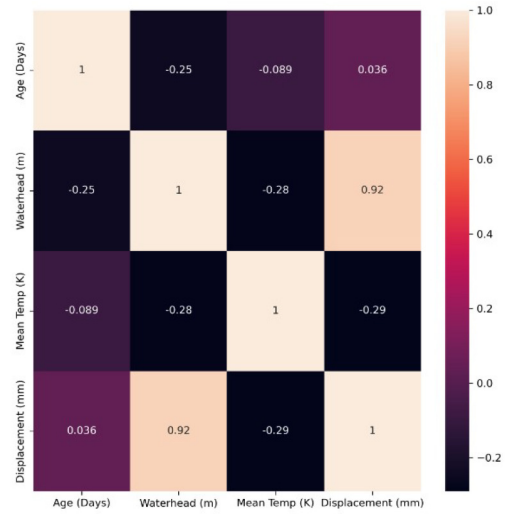


Fig. 3. Correlation matrix of variables.

The algorithms were developed for several combinations from the set of independent variables using all possible subsets of feature selection. Usually, the sequential feature selection is prioritized for creating input combinations. However, the former method is given priority in this study due to the fewer number of predictor variables. The first combination includes all three predictor variables for model development. The second, third and fourth input combinations include two predictor variables each, while the fifth, sixth and seventh combinations consist of only one predictor variable. The combination number was prioritized based on the value of correlation with dam displacement (δ) for the variable as seen from Fig. 3.

The variable waterhead has the maximum correlation with δ and is included in models second, third and fifth. The age of the dam has almost 0 correlation with δ and is used with waterhead and temperature in combination second and fourth respectively. It is used alone in combination sixth. Mean ambient temperature is used in third, fourth and seventh combinations due to its negative correlation with δ . The model developed are marked Y1-Y7 for their respective combination number. A generalized workflow for this study is shown in Fig. 4.

2.6. Statistical evaluation metrics

To assess the accuracy of prediction, several evaluation metrics were adopted including coefficient of determination (R^2), root mean square error (RMSE), mean absolute error (MAE), mean absolute percentage error (MAPE), Nash-Sutcliffe efficiency (NSE), and agreement index (MD). The expressions for

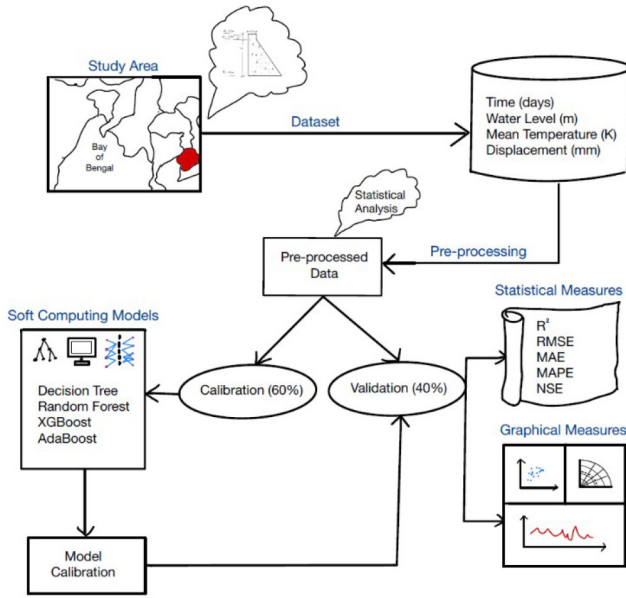


Fig. 4. Proposed workflow of study.

calculating these metrics are as follows:

$$R = \frac{\sum_{i=1}^n (y_{pi} - \bar{y}_p) (y_i - \bar{y})}{\sqrt{\sum_{i=1}^n (y_{pi} - \bar{y}_p)^2 \sum_{i=1}^n (y_i - \bar{y})^2}} \quad (10)$$

$$RMSE = \sqrt{\frac{\sum_{i=1}^n (y_{pi} - y_i)^2}{n}} \quad (11)$$

$$MAE = \frac{1}{n} \sum_{i=1}^n |y_{pi} - y_i| \quad (12)$$

$$MAPE = \frac{1}{n} \sum_{i=1}^n \frac{|y_{pi} - y_i|}{y_p} \quad (13)$$

$$NSE = 1 - \frac{\sum_{i=1}^n (y_{pi} - y_i)^2}{\sum_{i=1}^n (y_i - \bar{y})^2} \quad (14)$$

$$MD = 1 - \frac{\sum_{i=1}^n (y_{pi} - y_i)^2}{\sum_{i=1}^n (|y_{pi} - \bar{y}| + |y_i - \bar{y}|)^2} \quad (15)$$

where, n is the number of predicted samples, y , \bar{y} , y_p , and \bar{y}_p represent observed value, mean observed value, predicted value and mean value for prediction of dam displacement respectively. These evaluation metrics were adopted to infer various indicators of model validations.

3. Case study

3.1. Study area

The study revolves around a concrete gravity dam, RCCD located in Cambodia. It is a massive hydropower structure built across the Kamchay River with a total elevation of 153 m. The foundation is located around 112 m below it, at a height of 41 m above the mean sea level. The normal water level was initially kept at 133 m, but has been updated in April, 2011 to store the water up to the elevation of 150m. The geological study of the location informs that the bedrock below the structure is mainly comprised of quartz sandstone, and the rocks of the right flanks are also weak in strength. This also boosts the necessity of studying the displacement at different sections to understand the current status of foundation deformation. For measuring purposes, six inverted plumb lines were installed at elevations of 153 m, 120 m and 88 m. They were installed on either of the two flanks and are denoted as IP1, IP2, IP3, IP4, IP5 and IP6. In this study, we consider a section measured at 118.25 m with IP4 (near 120 m).

3.2. Dataset description

3.2.1. Basic theory

Owing to the complexity of dam displacement, the derivation of a casual relationship between dam displacement and its influential factors is almost impossible. Based on the present research findings, water pressure, ambient temperature, and time have the greatest effects on the dam's displacement [25, 62]. Consequently, the displacement of the dam (δ) can be written as a function of these factors: hydrostatic (δ_H), temperature (δ_T), and aging (δ_θ) with residual error ϵ .

$$\delta = \delta_H + \delta_T + \delta_\theta + \epsilon \quad (16)$$

The hydrostatic component of dam displacement consists of three subcomponents, name, the dam displacement by direct influence of hydrostatic pressure, the displacement of the dam body caused by foundation deformation under internal forces due to hydrostatic pressure, and the bedrock rotation caused by the vertical weight component of the water [26]. The hydrostatic component can be written as follows:

$$\delta_H = \sum_{i=1}^n a_i \Delta H^i \quad (17)$$

where, ΔH is the elevation difference in water level between the time of observation and the beginning of

observation, a is a fitting coefficient and n is a number that is equal to three for concrete gravity dams and four for arch dams.

The interior temperature field of the dam and the ambient temperature are related to the temperature variable. Furthermore, the continuity and integrity of the temperature monitoring data throughout the period are important considerations in the selection and computation of temperature variables [63]. The temperature variable can be expressed using the combination of harmonic period functions as follows when the temperature monitoring data are not continuous, insufficient, or unavailable:

$$\delta_T = \sum_{i=1}^2 \left[b_{1i} \left(\sin \left(\frac{2\pi it}{365} \right) - \sin \left(\frac{2\pi it_0}{365} \right) \right) + b_{2i} \left(\cos \left(\frac{2\pi it}{365} \right) - \cos \left(\frac{2\pi it_0}{365} \right) \right) \right] \quad (18)$$

where b is the regression coefficient, t is the cumulative number of days between observations and, t_0 is the first monitored day of the dataset from the first observation day, respectively. The value of i is 1 for the annual cycle and 2 for half yearly cycle [25].

The aging component can be used to grasp an idea about the creep of concrete in the dam body and bedrock and be written as follows:

$$\delta_\theta = c_1 \left(\frac{t - t_0}{100} \right) + c_2 \ln \left(\frac{t - t_0}{100} \right) \quad (19)$$

where, c_1 and c_2 are regression coefficients, with t and t_0 holding the same meaning as in equation Eq. (19). However, there is a nonlinear and delayed relationship between the displacements and the temperature and water level. Secondly, the time-varying effect is intricate and defies simplfunction description [46, 64].

3.2.2. Statistical analysis

A total of 170 samples were collected for the purpose of conducting this study at uneven intervals. The major part of dataset was retrieved from [40], and the ambient temperature data was collected from <https://www.ncei.noaa.gov/cdo-web/>. A thorough analysis of the dataset was also done to determine the statistical parameters of the dependent and independent variables and the correlation among them. The statistical analysis of the dataset is presented in Table 1.

Table 1 makes it evident that the ambient temperature in the region ranges from 295.93 K to 306.48 K. However, the IQR range depicts that most of the values lie between 301.48 K and 303.15 K. It can also be noted that the variables water head, temperature

Table 1. Statistical analysis of variables.

	Age (days)	Waterhead (m)	Mean temp (K)	Displacement (mm)
Minimum	1	13.83	295.93	29.41
Maximum	1377	31.71	306.48	35.91
Mean	645.99	26.64	302.16	33.94
Median	652	27.47	302.59	34.17
Q1	283	24.43	301.48	33.22
Q3	999.5	27.47	303.15	34.99
Range	1376	17.88	10.55	6.50
IQR Range	716.5	5.11	1.67	1.78
Standard deviation	410.10	4.03	1.70	1.38
Skewness	0.07	-1.11	-0.53	-1.00
Variance	168185	16.27	2.90	1.89
Kurtosis	-1.22	0.82	1.52	0.72

and displacement are negatively skewed and all four of the variables are platykurtic. Therefore, signifying the low tails in the distribution of data.

4. Results

4.1. Statistical evaluation

In this study, four regression models were employed for the prediction of dam deformation and six performance evaluators were used to assess their performance. The reason for opting to use six evaluators can be attributed to the fact that all the evaluation metrics have potential shortcomings and loopholes. Therefore, a grouped summary of six of them will produce acceptable metrics for further development. A summary of the results for DT, XGB, RF and ADB for the validation dataset is shown in Table 2.

Different models Y1-Y7 were calibrated on the same output variable by providing different sets of dataset combinations. The variation of input variables resulted in influencing the values of performance evaluation metrics. The seven models constructed in this study provided information about the sensitivity of dam displacement to different predictor variables and their respective combinations. It is evident from Table 2 that the XGB model marks the best outcome by implementing its ability to minimize the loss function. Conversely, RF surpasses XGB when it comes to models Y3 and Y5. It was previously introduced that in model Y5, the dependent variable is a function of the waterhead in the dam, whereas it consists of both the waterhead and age in Y3. ADB also performs better than XGB on the Y3 combination. This can be used to infer that RF prediction depends more on the variation of waterhead when compared to other algorithms. NSE indicates the predictive accuracy, and XGB for combination Y2 performs the best among all models and their combinations. The negative value

Table 2. Summary table of performance evaluation metrics.

Decision Tree Regression						
Model	R ²	RMSE	MAE	MAPE	NSE	MD
Y1	0.867	0.502	0.391	1.164	0.862	0.964
Y2	0.891	0.450	0.362	1.080	0.889	0.971
Y3	0.688	0.764	0.550	1.636	0.682	0.905
Y4	0.656	0.845	0.572	1.716	0.610	0.899
Y5	0.731	0.726	0.574	1.699	0.712	0.922
Y6	0.766	0.678	0.478	1.430	0.749	0.935
Y7	0.123	1.316	1.002	3.001	0.054	0.520
Extreme Gradient Boost Regression						
Model	R ²	RMSE	MAE	MAPE	NSE	MD
Y1	0.953	0.299	0.243	0.723	0.944	0.987
Y2	0.960	0.275	0.231	0.683	0.955	0.989
Y3	0.720	0.731	0.582	1.727	0.681	0.919
Y4	0.737	0.719	0.503	1.509	0.708	0.925
Y5	0.761	0.684	0.550	1.625	0.743	0.932
Y6	0.756	0.691	0.486	1.457	0.730	0.931
Y7	0.123	1.316	1.005	3.010	-1.543	0.520
Random Forests Regression						
Model	R ²	RMSE	MAE	MAPE	NSE	MD
Y1	0.894	0.453	0.359	1.070	0.888	0.967
Y2	0.900	0.434	0.354	1.052	0.897	0.971
Y3	0.813	0.589	0.451	1.341	0.811	0.945
Y4	0.656	0.915	0.704	2.107	0.543	0.775
Y5	0.813	0.587	0.464	1.374	0.812	0.946
Y6	0.667	0.864	0.660	1.978	0.593	0.819
Y7	0.144	1.260	0.976	2.920	0.134	0.485
AdaBoost Regression						
Model	R ²	RMSE	MAE	MAPE	NSE	MD
Y1	0.869	0.501	0.410	1.223	0.863	0.961
Y2	0.892	0.457	0.379	1.132	0.886	0.968
Y3	0.742	0.687	0.551	1.638	0.742	0.921
Y4	0.719	0.857	0.707	2.079	0.599	0.878
Y5	0.744	0.689	0.555	1.648	0.741	0.925
Y6	0.703	0.853	0.679	1.996	0.603	0.882
Y7	0.112	1.336	1.066	3.152	0.025	0.477

of NSE for the Y7 combination of XGB indicates that the average observed data would have been better than keeping the mean temperature as a predictor for model calibration. The value of MD represents the minimal deviation from the performance. XGB and DT have a value of MD greater than 0.9 for all 6 combinations excluding Y7. ADB also has relatively low values of deviation when compared with RF.

4.2. Graphical evaluation

Fig. 5 illustrates the scatter plot for the Y1 combination of all four soft computing models. The value of R² for the Y1 combination that includes all three predictor variables is maximum for XGB (0.9527), followed by RF (0.8839), whereas ADB and DT show values for R² of 0.8776 and 0.8698 respectively. Figs. 6 to 9

shows the scatter plot for models Y2-Y7 for DT, XGB, RF and ADB respectively under the testing phase. R² is a measure to understand the proportion of variance in the predicted variable. For the decision tree model algorithm depicted in Fig. 6, the Y2 model performs the best with an R² score of 0.8860 which is followed by Y6, Y5, Y3, and Y4.

Model Y7 based on only mean temperature is unable to predict displacement for any of the four algorithms considered in this study (R² < 0.2). As for the scatter plot of XGB shown in Fig. 7, Y2 performs the best with the coefficient of the determination being 0.9595, which is followed by models Y5, Y6, Y4 and Y3.

In the case of RF (Fig. 8), Y2 (R² = 0.8998) is followed by Y5 and Y3, then Y6 with Y4 showing a very moderate value of R². The variation of R² in RF bears intriguing results as the difference between the Y3 and Y6 is approximately 0.1, and between the models Y3 with Y4 is over 0.2. This decrement of over 20% between Y3 and Y4 emerged on the substitution of waterhead with mean temperature.

The plot for ADB (Fig. 9) indicates that the Y2 model (R² = 0.8926) is succeeded by Y5 and Y3 in the prediction of displacement. Y4 and Y6 depicted a value of around 0.7 for coefficient of determination. However, the influence of outliers on R² is an important aspect and should be taken as a heed to visualize using other means as well.

The line chart is a great means of visualizing the error that occurred in prediction. Fig. 10 depicts the variation of displacement with time (aging effect on dam displacement) for Y1 models of different algorithms. It can be visualized that model Y1 in XGB performs much better when compared to the others. This is also supported by its MAE and RMSE values of 0.243 and 0.299 respectively. The performance evaluation of DT is more complex as it has better indices when it comes to MAE, MAPE and MD. However, it is evident from Fig. 10 that the DT model is overfitting as it is making sharp cuts which might correspond more to the validation datasets. On the other hand, ADB is under fitting in the case of combination Y1. It is not able to find the peak displacements and rather depicts a smoother transition when studied under the time duration of about 350–700 days after the first observation. RF prediction is playing closer to the actual displacement value remains usually a bit lower than the observed value.

Figs. 11 to 14 shows the displacement variation as a function of age for DT, XGB, RF and ADB respectively. In Fig. 11, it is evident that Y2 and Y6 predictions follow the validation data very closely. They also bear the lowest value for RMSE, MAE and MAPE. The value of these three performance metrics for model Y6 is

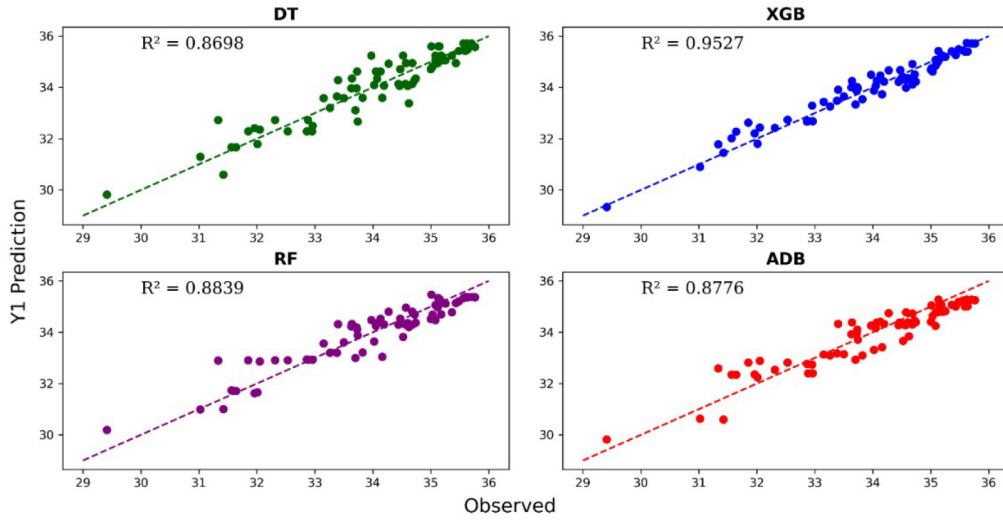


Fig. 5. Prediction performance Y1 model.

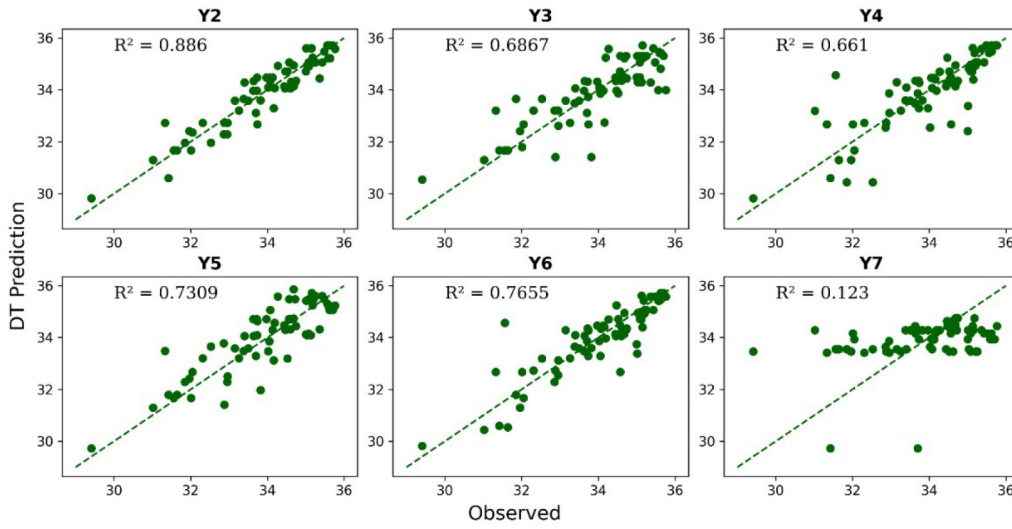


Fig. 6. Performance of DT prediction (Y2-Y7).

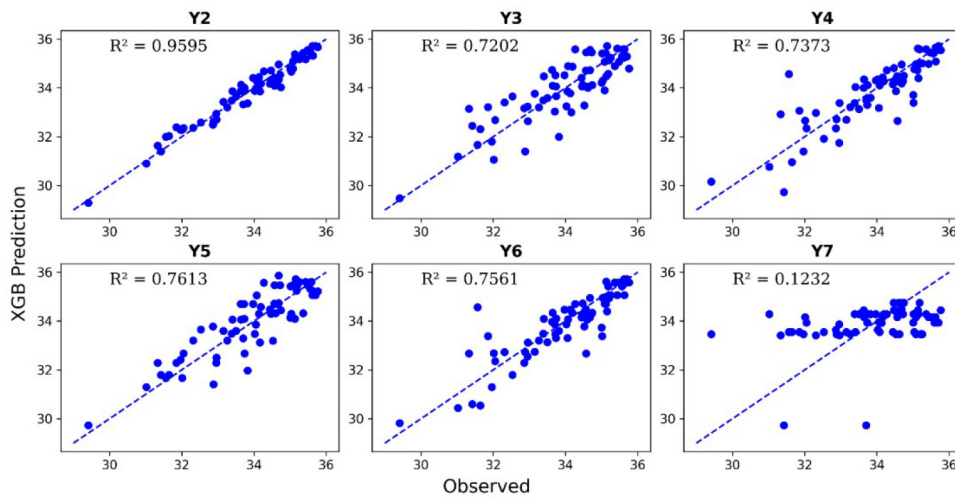


Fig. 7. Performance of XGB prediction (Y2-Y7).

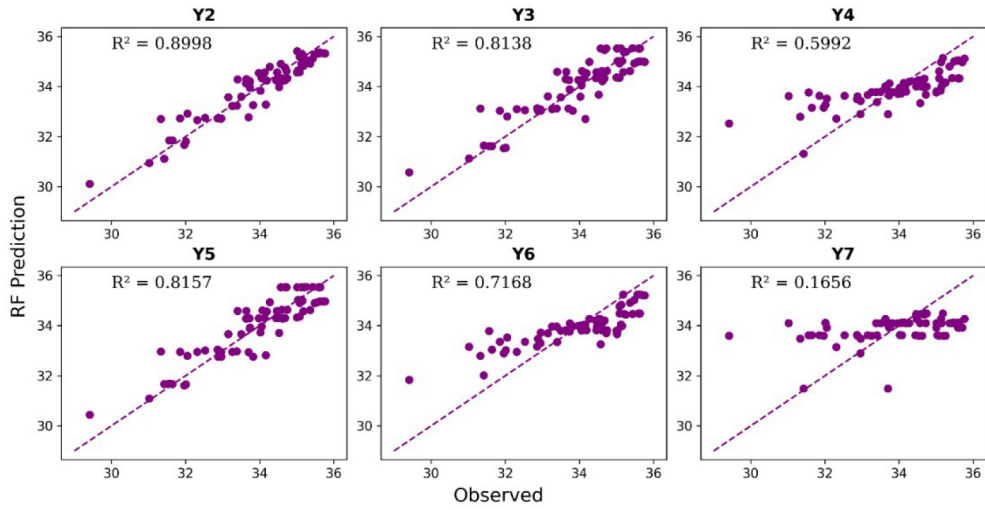


Fig. 8. Performance of RF prediction (Y2-Y7).

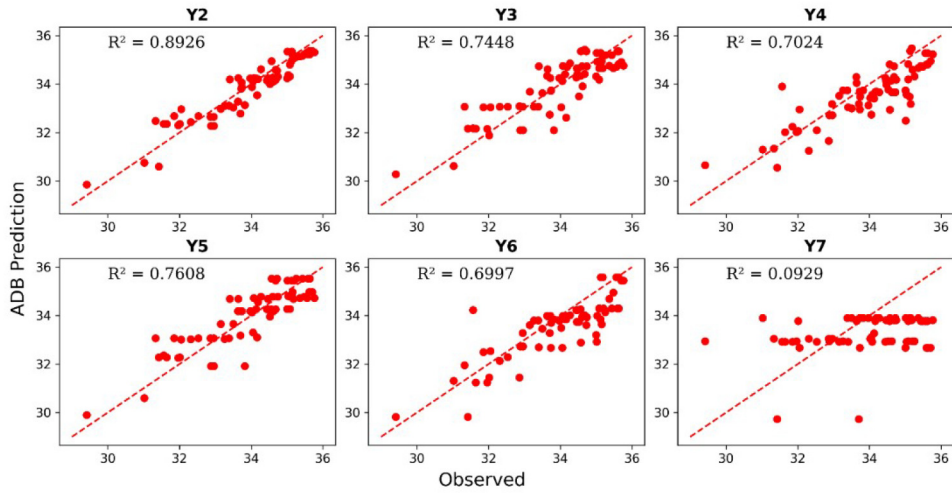


Fig. 9. Performance of ADB prediction (Y2-Y7).

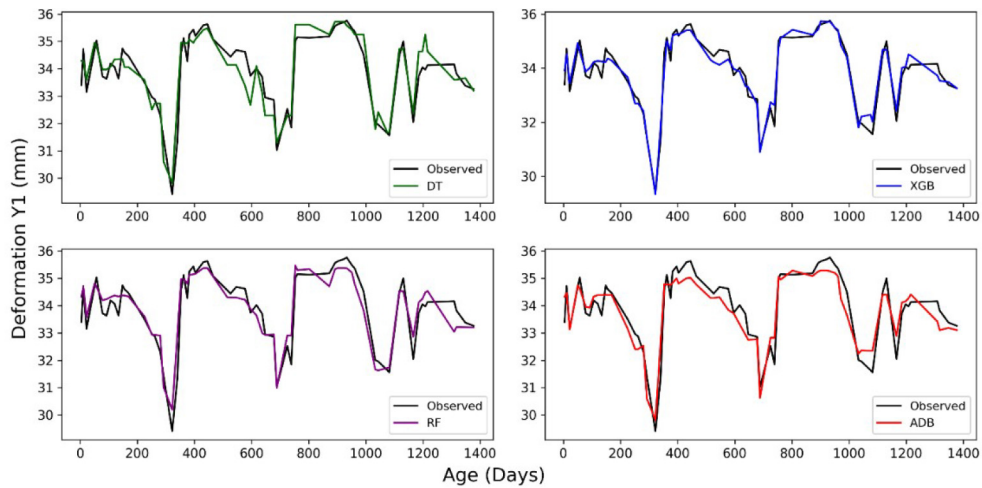


Fig. 10. Deformation vs aging plot for Y1 model.

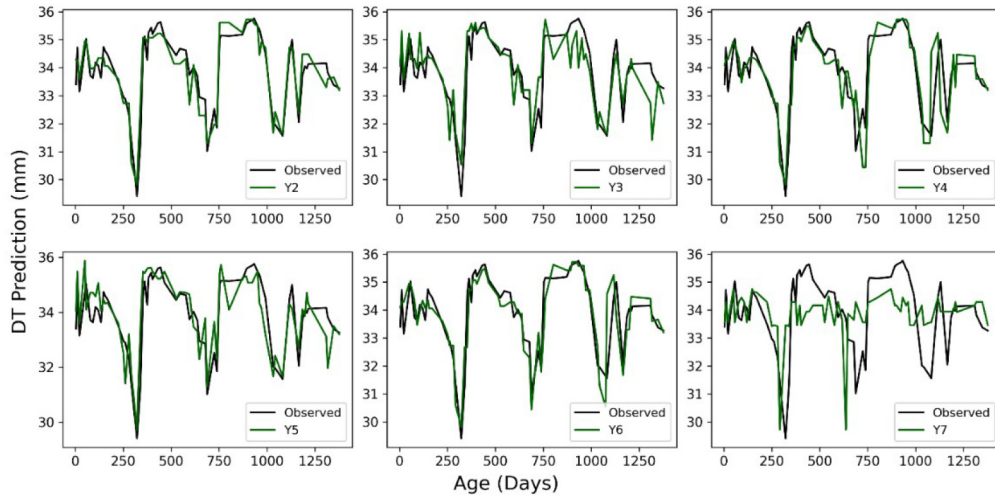


Fig. 11. Displacement vs aging plot for DT (Y2-Y7).

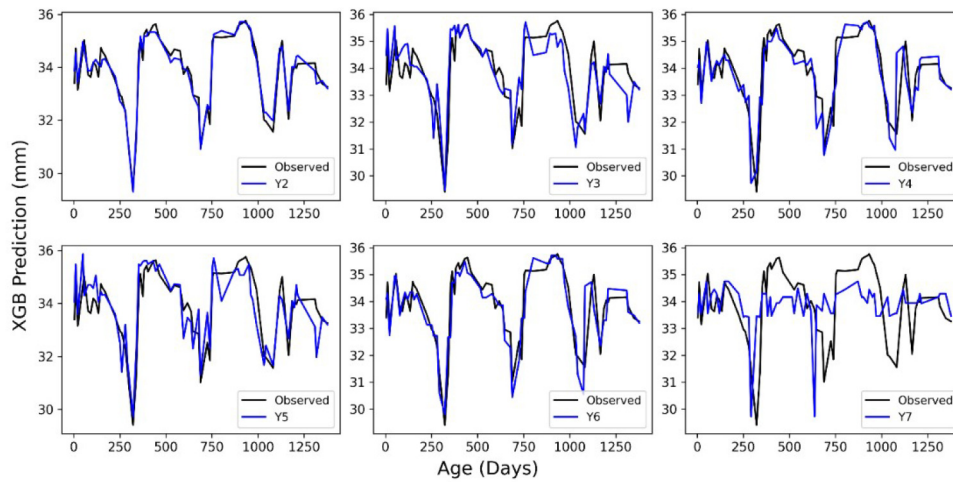


Fig. 12. Displacement vs aging plot for XGB (Y2-Y7).

the least for DT, with the numerical value of 0.678, 0.478 and 1.430 respectively. These three metrics are regarded as a sound methodology for measuring the difference between predicted and observed values.

The Y2 model of XGB has the best results among all the models developed in this study. It provides a very accurate measure of the result, with the minimum RMSE and MAE values of 0.275 and 0.231 respectively. The value of MAE for Y6 is less than its counterpart of Y5. Conversely, the model Y6 lies behind Y5 in terms of other evaluation metrics. However, it can also be seen from Fig. 12 that the Y6 model is sounder when it is compared to Y5 for an accurate measure of peak displacements of the dam. Meanwhile, the RF prediction is only acceptable for models Y2, Y3 and Y5 as visualized from Fig. 13. It is interesting to note that all three of these models have a common independent variable waterhead. RF also

has the lowest MAE and RMSE values of 0.451 and 0.589 for Y3 and 0.464 and 0.587 for Y5 respectively. The Y4 and Y6 models of RF depict underfitting of data and might improve for a greater number of training datasets.

ADB line plot between displacement and aging has been illustrated in Fig. 14. The ADB prediction is similar to RF and shows better results for Y3 and Y5 after model Y2. Although the Y5 model performs the second best in terms of evaluation metrics, it can be witnessed from the line chart that it under fits for the second deformation peak that occurred during the study period.

Taylor diagram is a visual representation [65] created using three metrics: standard deviation, statistical correlation, and RMSE to illustrate the whereabouts of the predicted value of the models with respect to the observed value. Fig. 15 contains

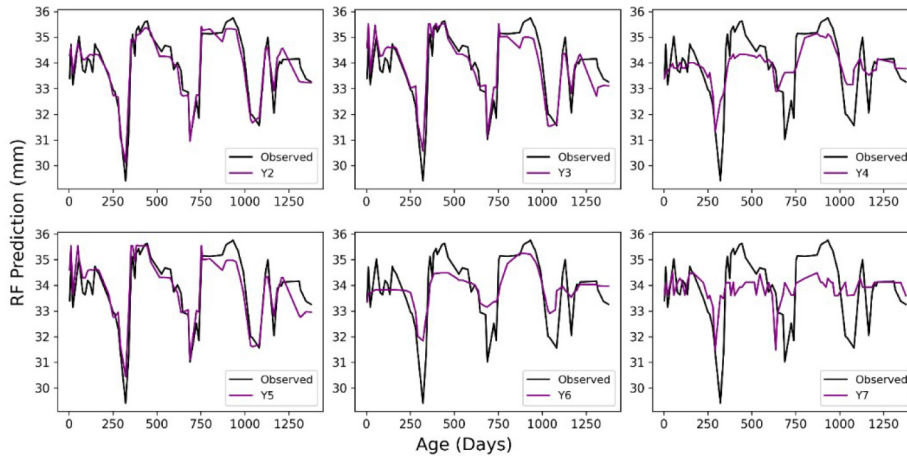


Fig. 13. Displacement vs aging plot for RF (Y2-Y7).

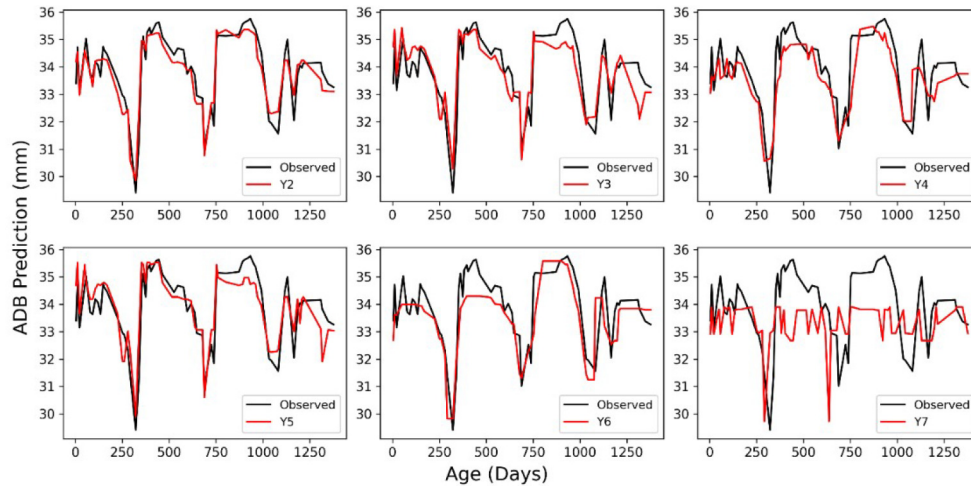


Fig. 14. Displacement vs aging plot for ADB (Y2-Y7).

the Taylor representation for all four algorithms. Owing to the limitations of any evaluation metric, the Taylor chart is widely accepted due to its ability to represent three metrics at the same time. It is evident that model Y2 of XGB has the least distance to the actual value, and therefore produces the most accurate prediction of dam displacement and is followed closely by model Y1 of XGB. Models Y1 and Y2 of all four algorithms are within the first radial circle of 0.5 RMSE. The Y3 and Y5 models also lie very close to the first circle and can be considered for prediction on limited data availability. However, the models Y4 and Y6 of RF are far from the actual value. It can be inferred from the Taylor chart that all the models provided acceptable results except Y7 of all algorithms, which depicted low value of statistical correlation and deviation, and a high value of RMSE. The Taylor chart also perceived the superiority of using waterhead and age as predictor variables.

5. Discussion

Application of ML algorithms to counter the complex problems in hydraulic structures is the need of the hour as these methods are accurate in simulating the non-linear relationships between dependent and independent variables. In this study, it was noted that the model Y2 performs the best for every algorithm. This result could be attributed to the fact that perhaps the models began to overfit on adding the ambient temperature combinations in Y1. All four algorithms were able to provide satisfactory results with XGB providing the best result for the Y1, Y2 and Y4 models. Whereas, RF dominates the result for the Y3 and Y5 models, and DT depicts the best prediction on the Y6 model. This signifies the different datasets that could acquire acceptable results. In the presence of an ample amount of datasets, XGB is the most preferred algorithm out of the four ML models tested in this

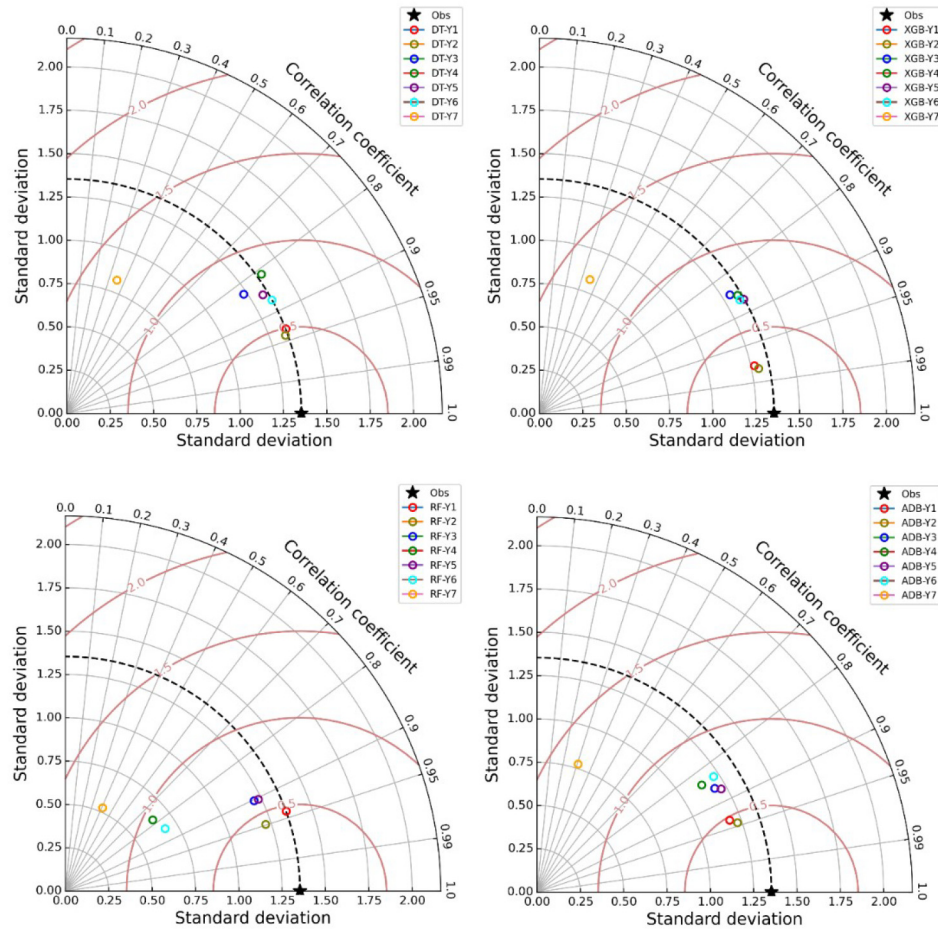


Fig. 15. Taylor representation of ML models for the testing phase.

study. Since RF has an R^2 value greater than 0.8 for every combination including waterhead level, it can be inferred that this algorithm is greatly influenced by the presence of accurate measures of waterhead and can be used to predict dam displacement when only waterhead level observation is available. Conversely, it shows a low value of 0.656 and 0.667 for models Y4 and Y6 respectively. This implies that its reliability is compromised when aging is considered the major factor for dam deformation prediction. Whereas XGB and DT provided acceptable results with aging as predictor variables. DT performed the best in the situation when only the age of the dam was available as the predictor variable. Therefore, it can be used to predict the dam displacement effectively in case of the most abundant data available easily. Mean ambient temperature turned out to be a negative influence on the prediction models in this study. However, an interesting conclusion can be inferred that ADB is the algorithm that prevented the deterioration of its result even with the addition of an unwanted predictor variable in limited data availabil-

ity (in the case of Y4 and Y6). This justifies the ability of ADB to adjust the weights during model build-up and avoid negative influence by the unwanted independent variables. It should be noted that the MAE value of DT prediction is less when compared to ADB. Conversely, the superiority of ADB over DT is evident from the higher value of the coefficient of determination R^2 . This information can be used to infer that we cannot barely rely on MAE for performance evaluation as it was practiced by [46] for their improved RF model. This can also be used to induce the requirement of using multiple evaluation measures for model validation. Although the temperature influence did not provide expected results, this one case study cannot be used to rule out the effect of temperature as noted by previous research [66, 67]. However, these studies indicated long term temperature induced effects on dam displacement. As a result, it can be inferred that unevenly distributed limited ambient air temperature data might not be the best predictor variable to be included in similar studies.

6. Conclusion

The development of reliable models for the prediction of dam displacement is a need of the hour. This study worked on establishing different ML models for the prediction of dam displacement in limited data availability. A total of 170 observations collected from previous work were divided in a 60:40 ratio for calibration and validation purposes, implying that model training was done using only 102 observations, suggesting the superiority of ensemble models to predict displacement on minuscule amounts of data, and their reliability over conventional statistical methods. Seven input combinations were created based on the availability of datasets and were used to test the reliability of ML algorithms for displacement prediction using feature selection approach. The validation was done through statistical and graphical metrics. The results depicted that different algorithms should be deployed according to the variation in data availability. Models Y1, Y2 and Y4 performed the best for XGB, while models Y3 and Y5 were more reliable in case of RF, with DT leading the charge for Y6 model. The primary conclusions inferred from this study can be summarized as follows:

- i. The XGB model performed exceptionally well in the availability of comprehensive datasets. Its prediction for displacement based on aging also provided acceptable results ($R^2 > 0.7$).
- ii. RF model prediction is greatly influenced by the amount of water present in the dam. Its reliability is degraded immensely on removing waterhead from the set of predictor variables.
- iii. Conventional DT algorithm reported acceptable results, especially in the presence of age datasets. Moreover, DT is a time-efficient means of prediction and utilizes less computational power.
- iv. ADB provided results which were unaffected by the presence of a variable that had a negative influence in the later combinations.

Although this study verified the time-induced effects on dam displacement, there is still room for refinement. Attention mechanisms should be integrated with these ensemble models to further verify their integrity on specific datasets. Time induced effect on displacement should be further analyzed for trend by integrating Mann-Kendall and Theil-Sen slope estimates. The generalization ability and prediction resilience of the models employed in this study will be enhanced with further monitoring data from various types of concrete dams in long-term service.

Conflict of interest: The authors declare no conflict of interest to any party.

References

1. F. Pearce, "When the levees break," *Science*, vol. 372, pp. 676–9, 1979) 2021, doi:10.1126/science.372.6543.676.
2. V. Hermoso, M. Clavero, and A. J. Green, "Don't let damage to wetlands cancel out the benefits of hydropower," *Nature*, vol. 568, pp. 171–171, 2019, doi:10.1038/d41586-019-01140-7.
3. G. Prakash, A. Sadhu, S. Narasimhan, and J.-M. Brehe, "Initial service life data towards structural health monitoring of a concrete arch dam," *Struct Control Health Monit*, vol. 25, p. e2036, 2018, doi:10.1002/stc.2036.
4. A. P. Phyto, H. Yabar, and D. Richards, "Managing dam breach and flood inundation by hec-ras modeling and gis mapping for disaster risk management," *Case Studies in Chemical and Environmental Engineering*, vol. 8, p. 100487, 2023, doi:10.1016/j.cscee.2023.100487.
5. C. Jia, Y. Li, and Q. Ren, "Cracking analysis of high concrete gravity dams under floodwater and seismic effects," in *2010 Asia-Pacific Power and Energy Engineering Conference, IEEE*, 2010, pp. 1–4, doi:10.1109/APPEEC.2010.5449345.
6. G. Yang, J. Sun, J. Zhang, J. Niu, B. Luan, Z. Huang *et al.*, "Research on temperature control index for high concrete dams based on information entropy and cloud model from the view of spatial field," *Water (Basel)*, vol. 15, p. 4023, 2023, doi:10.3390/w15224023.
7. X. Yu, J. Li, and F. Kang, "A hybrid model of bald eagle search and relevance vector machine for dam safety monitoring using long-term temperature," *Advanced Engineering Informatics*, vol. 55, p. 101863, 2023, doi:10.1016/j.aei.2022.101863.
8. S. Chen, C. Gu, C. Lin, E. Zhao, and J. Song, "Safety monitoring model of a super-high concrete dam by using rbf neural network coupled with kernel principal component analysis," *Math Probl Eng*, vol. 2018, pp. 1–13, 2018, doi:10.1155/2018/1712653.
9. E. Mavhura, "Dam-induced displacement and resettlement: Reflections from tokwe-mukorsi flood disaster, zimbabwe," *International Journal of Disaster Risk Reduction*, vol. 44, p. 101407, 2020, doi:10.1016/j.ijdrr.2019.101407.
10. F. Vahedifard, K. Madani, A. AghaKouchak, and S. K. Thota, "Preparing for proactive dam removal decisions," *Science*, vol. 369, pp. 150–150, 1979) 2020, doi:10.1126/science.abc9953.
11. M. Ishfaq, Q. Dai, A. Wahid, B. Saddique, K. Z. Jadoon, H. T. Janjuhah *et al.*, "Trend analysis of hydro-climatological parameters and assessment of climate impact on dam seepage using statistical and machine learning models," *Environ Earth Sci*, vol. 82, p. 542, 2023, doi:10.1007/s12665-023-11216-3.
12. H. Tabari, "Climate change impact on flood and extreme precipitation increases with water availability," *Sci Rep*, vol. 10, p. 13768, 2020, doi:10.1038/s41598-020-70816-2.
13. D. Yuan, C. Gu, X. Qin, C. Shao, and J. He, "Performance-improved tsvr-based dhm model of super high arch dams using measured air temperature," *Eng Struct*, vol. 250, p. 113400, 2022, doi:10.1016/j.engstruct.2021.113400.
14. M. Li, M. Li, Q. Ren, H. Li, and L. Song, "Drlstm: A dual-stage deep learning approach driven by raw monitoring data for dam displacement prediction," *Advanced Engineering Informatics*, vol. 51, p. 101510, 2022, doi:10.1016/j.aei.2021.101510.
15. M. Li, Y. Shen, Q. Ren, and H. Li, "A new distributed time series evolution prediction model for dam deformation based on constituent elements," *Advanced Engineering Informatics*, vol. 39, pp. 41–52, 2019, doi:10.1016/j.aei.2018.11.006.

16. S. Wang, Y. Xu, C. Gu, Q. Xia, and K. Hu, "Two spatial association-considered mathematical models for diagnosing the long-term balanced relationship and short-term fluctuation of the deformation behaviour of high concrete arch dams," *Struct Health Monit*, vol. 19, pp. 1421–39, 2020, doi:[10.1177/1475921719884861](https://doi.org/10.1177/1475921719884861).
17. B. Chen, T. Hu, Z. Huang, and C. Fang, "A spatio-temporal clustering and diagnosis method for concrete arch dams using deformation monitoring data," *Struct Health Monit*, vol. 18, pp. 1355–71, 2019, doi:[10.1177/1475921718797949](https://doi.org/10.1177/1475921718797949).
18. J. Li, Z. Wu, J. Chen, X. Lu, and Z. Li, "Fem-bayesian kriging method for deformation field estimation of earth dams with limited monitoring data," *Comput Geotech*, vol. 148, p. 104782, 2022, doi:[10.1016/j.compgeo.2022.104782](https://doi.org/10.1016/j.compgeo.2022.104782).
19. F. Salazar, R. Morán, M. Á. Toledo, and E. Oñate, "Data-based models for the prediction of dam behaviour: A review and some methodological considerations," *Archives of Computational Methods in Engineering*, vol. 24, pp. 1–21, 2017, doi:[10.1007/s11831-015-9157-9](https://doi.org/10.1007/s11831-015-9157-9).
20. L. Wen, J. Chai, Z. Xu, Y. Qin, and Y. Li, "A statistical review of the behaviour of concrete-face rockfill dams based on case histories," *Géotechnique*, vol. 68, pp. 749–71, 2018, doi:[10.1680/jgeot.17.P.095](https://doi.org/10.1680/jgeot.17.P.095).
21. Y. Jia, B. Xu, S. Chi, B. Xiang, D. Xiao, and Y. Zhou, "Joint back analysis of the creep deformation and wetting deformation parameters of soil used in the guanyinyan composite dam," *Comput Geotech*, vol. 96, pp. 167–77, 2018, doi:[10.1016/j.compgeo.2017.10.018](https://doi.org/10.1016/j.compgeo.2017.10.018).
22. B. Wei, B. Liu, D. Yuan, Y. Mao, and S. Yao, "Spatiotemporal hybrid model for concrete arch dam deformation monitoring considering chaotic effect of residual series," *Eng Struct*, vol. 228, p. 111488, 2021, doi:[10.1016/j.engstruct.2020.111488](https://doi.org/10.1016/j.engstruct.2020.111488).
23. J. Pan, W. Liu, C. Liu, and J. Wang, "Convolutional neural network-based spatiotemporal prediction for deformation behavior of arch dams," *Expert Syst Appl*, vol. 232, p. 120835, 2023, doi:[10.1016/j.eswa.2023.120835](https://doi.org/10.1016/j.eswa.2023.120835).
24. J. Mata, "Interpretation of concrete dam behaviour with artificial neural network and multiple linear regression models," *Eng Struct*, vol. 33, pp. 903–10, 2011, doi:[10.1016/j.engstruct.2010.12.011](https://doi.org/10.1016/j.engstruct.2010.12.011).
25. Z. Wen, R. Zhou, and H. Su, "Mr and stacked grus neural network combined model and its application for deformation prediction of concrete dam," *Expert Syst Appl*, vol. 201, p. 117272, 2022, doi:[10.1016/j.eswa.2022.117272](https://doi.org/10.1016/j.eswa.2022.117272).
26. Q. Ren, M. Li, H. Li, L. Song, W. Si, and H. Liu, "A robust prediction model for displacement of concrete dams subjected to irregular water-level fluctuations," *Computer-Aided Civil and Infrastructure Engineering*, vol. 36, pp. 577–601, 2021, doi:[10.1111/mice.12654](https://doi.org/10.1111/mice.12654).
27. F. Kang, X. Liu, and J. Li, "Temperature effect modeling in structural health monitoring of concrete dams using kernel extreme learning machines," *Struct Health Monit*, vol. 19, pp. 987–1002, 2020, doi:[10.1177/1475921719872939](https://doi.org/10.1177/1475921719872939).
28. B. Li, J. Yang, and D. Hu, "Dam monitoring data analysis methods: A literature review," *Struct Control Health Monit*, vol. 27, 2020, doi:[10.1002/stc.2501](https://doi.org/10.1002/stc.2501).
29. S. Wang, C. Xu, C. Gu, H. Su, K. Hu, and Q. Xia, "Displacement monitoring model of concrete dams using the shape feature clustering-based temperature principal component factor," *Struct Control Health Monit*, vol. 27, 2020, doi:[10.1002/stc.2603](https://doi.org/10.1002/stc.2603).
30. J. Tian, Y. Luo, X. Lu, Y. Li, and J. Chen, "Physical data-driven modeling of deformation mechanism constraints on earth-rock dams based on deep feature knowledge distillation and finite element method," *Eng Struct*, vol. 307, p. 117899, 2024, doi:[10.1016/j.engstruct.2024.117899](https://doi.org/10.1016/j.engstruct.2024.117899).
31. X. Liu, Z. Li, L. Sun, E. Y. Khailah, J. Wang, and W. Lu, "A critical review of statistical model of dam monitoring data," *Journal of Building Engineering*, vol. 80, p. 108106, 2023, doi:[10.1016/j.jobe.2023.108106](https://doi.org/10.1016/j.jobe.2023.108106).
32. A. Parsaie, "Predictive modeling the side weir discharge coefficient using neural network," *Model Earth Syst Environ*, vol. 2, p. 63, 2016, doi:[10.1007/s40808-016-0123-9](https://doi.org/10.1007/s40808-016-0123-9).
33. J. Tian, C. Chen, X. Lu, Y. Li, and J. Chen, "Deep transfer learning-based time-varying model for deformation monitoring of high earth-rock dams," *Eng Appl Artif Intell*, vol. 138, p. 109310, 2024, doi:[10.1016/j.engappai.2024.109310](https://doi.org/10.1016/j.engappai.2024.109310).
34. J. Tian, Y. Luo, X. Lu, Y. Li, and J. Chen, "Physical data-driven modeling of deformation mechanism constraints on earth-rock dams based on deep feature knowledge distillation and finite element method," *Eng Struct*, vol. 307, p. 117899, 2024, doi:[10.1016/j.engstruct.2024.117899](https://doi.org/10.1016/j.engstruct.2024.117899).
35. Y. Su, J. Fu, C. Lin, X. Lai, Z. Zheng, Y. Lin *et al.*, "A novel deep learning multi-step prediction model for dam displacement using chrono-initialized lstm and sequence-to-sequence framework," *Expert Syst Appl*, vol. 271, p. 126624, 2025, doi:[10.1016/j.eswa.2025.126624](https://doi.org/10.1016/j.eswa.2025.126624).
36. V. Ranković, N. Grujović, D. Divac, and N. Milivojević, "Development of support vector regression identification model for prediction of dam structural behaviour," *Structural Safety*, vol. 48, pp. 33–9, 2014, doi:[10.1016/j.strusafe.2014.02.004](https://doi.org/10.1016/j.strusafe.2014.02.004).
37. M.-Y. Cheng, M.-T. Cao, and I.-F. Huang, "Hybrid artificial intelligence-based inference models for accurately predicting dam body displacements: A case study of the fei tsui dam," *Struct Health Monit*, vol. 21, pp. 1738–56, 2022, doi:[10.1177/14759217211044116](https://doi.org/10.1177/14759217211044116).
38. S. Luo, B. Wei, and L. Chen, "Multi-point deformation monitoring model of concrete arch dam based on mvmd and 3d-cnn," *Appl Math Model*, vol. 125, pp. 812–26, 2024, doi:[10.1016/j.apm.2023.10.030](https://doi.org/10.1016/j.apm.2023.10.030).
39. H. Gu, M. Yang, C. Gu, and X. Huang, "A factor mining model with optimized random forest for concrete dam deformation monitoring," *Water Science and Engineering*, vol. 14, pp. 330–6, 2021, doi:[10.1016/j.wse.2021.10.004](https://doi.org/10.1016/j.wse.2021.10.004).
40. C. Lin, T. Li, S. Chen, X. Liu, C. Lin, and S. Liang, "Gaussian process regression-based forecasting model of dam deformation," *Neural Comput Appl*, vol. 31, pp. 8503–18, 2019, doi:[10.1007/s00521-019-04375-7](https://doi.org/10.1007/s00521-019-04375-7).
41. J. Zhang, X. Cao, J. Xie, and P. Kou, "An improved long short-term memory model for dam displacement prediction," *Math Probl Eng*, vol. 2019, pp. 1–14, 2019, doi:[10.1155/2019/6792189](https://doi.org/10.1155/2019/6792189).
42. T. Lu, C. Gu, D. Yuan, K. Zhang, and C. Shao, "Deep learning model for displacement monitoring of super high arch dams based on measured temperature data," *Measurement*, vol. 222, p. 113579, 2023, doi:[10.1016/j.measurement.2023.113579](https://doi.org/10.1016/j.measurement.2023.113579).
43. C. Molnar, G. Casalicchio, and B. Bischl, "Interpretable machine learning – a brief history," *State-of-the-Art and Challenges*, pp. 417–31, 2020, doi:[10.1007/978-3-030-65965-3_28](https://doi.org/10.1007/978-3-030-65965-3_28).
44. P. Linardatos, V. Papastefanopoulos, and S. Kotsiantis, "Explainable ai: A review of machine learning interpretability methods," *Entropy*, vol. 23, p. 18, 2020, doi:[10.3390/e23010018](https://doi.org/10.3390/e23010018).
45. F. Salazar, M. Á. Toledo, E. Oñate, and B. Suárez, "Interpretation of dam deformation and leakage with boosted regression trees," *Eng Struct*, vol. 119, pp. 230–51, 2016, doi:[10.1016/j.engstruct.2016.04.012](https://doi.org/10.1016/j.engstruct.2016.04.012).

46. Y. Su, K. Weng, C. Lin, and Z. Zheng, "An improved random forest model for the prediction of dam displacement," *IEEE Access*, vol. 9, pp. 9142–53, 2021, doi:[10.1109/ACCESS.2021.3049578](https://doi.org/10.1109/ACCESS.2021.3049578).
47. Q. Wang, Z. Tian, X. Chen, and S. Zhai, "Research on dam deformation prediction based on variable weight combination model," in *2024 4th International Conference on Neural Networks, Information and Communication (NNICE)*, IEEE, 2024, pp. 900–3, doi:[10.1109/NNICE61279.2024.10498648](https://doi.org/10.1109/NNICE61279.2024.10498648).
48. L. Wen, Y. Li, W. Zhao, W. Cao, and H. Zhang, "Predicting the deformation behaviour of concrete face rockfill dams by combining support vector machine and adaboost ensemble algorithm," *Comput Geotech*, vol. 161, p. 105611, 2023, doi:[10.1016/j.compgeo.2023.105611](https://doi.org/10.1016/j.compgeo.2023.105611).
49. M. Liu, Z. Wen, and H. Su, "Deformation prediction based on denoising techniques and ensemble learning algorithms for concrete dams," *Expert Syst Appl*, vol. 238, p. 122022, 2024, doi:[10.1016/j.eswa.2023.122022](https://doi.org/10.1016/j.eswa.2023.122022).
50. M. A. Ganaie, M. Hu, A. K. Malik, M. Tanveer, and P. N. Suganthan, "Ensemble deep learning: A review," *Eng Appl Artif Intell*, vol. 115, p. 105151, 2022, doi:[10.1016/j.engappai.2022.105151](https://doi.org/10.1016/j.engappai.2022.105151).
51. Z. Cao, Z. Li, J. Zhang, and H. Fu, "A homogeneous stacking ensemble learning model for fault diagnosis of rotating machinery with small samples," *IEEE Sens J*, vol. 22, pp. 8944–59, 2022, doi:[10.1109/JSEN.2022.3163760](https://doi.org/10.1109/JSEN.2022.3163760).
52. J. Lee, J. Kim, and W. Ko, "Day-ahead electric load forecasting for the residential building with a small-size dataset based on a self-organizing map and a stacking ensemble learning method," *Applied Sciences*, vol. 9, p. 1231, 2019, doi:[10.3390/app9061231](https://doi.org/10.3390/app9061231).
53. S. Suthaharan, "Decision tree learning," *p*, pp. 237–69, 2016, doi:[10.1007/978-1-4899-7641-3_10](https://doi.org/10.1007/978-1-4899-7641-3_10).
54. W. Chen, K. Fu, J. Zuo, X. Zheng, T. Huang, and W. Ren, "Radar emitter classification for large data set based on weighted-xgboost," *IET Radar, Sonar & Navigation*, vol. 11, pp. 1203–7, 2017, doi:[10.1049/iet-rsn.2016.0632](https://doi.org/10.1049/iet-rsn.2016.0632).
55. W. P. Zhao, J. Li, J. Zhao, D. Zhao, J. Lu, and X. Wang, "Xgb modelâ€: Research on evaporation duct height prediction based on xgboost algorithm," *Radioengineering*, vol. 29, pp. 81–93, 2020, doi:[10.13164/re.2020.0081](https://doi.org/10.13164/re.2020.0081).
56. B. L. R. Forests, "Mach learn," vol. 45, pp. 5–32, 2001, doi:[10.1023/A:1010933404324](https://doi.org/10.1023/A:1010933404324).
57. G. N. Zaimes, D. Gounaridis, and E. Symeonakis, "Assessing the impact of dams on riparian and deltaic vegetation using remotely-sensed vegetation indices and random forests modelling," *Ecol Indic*, vol. 103, pp. 630–41, 2019, doi:[10.1016/j.ecolind.2019.04.047](https://doi.org/10.1016/j.ecolind.2019.04.047).
58. A. Belmokre, M. K. Mihoubi, and D. Santillan, "Seepage and dam deformation analyses with statistical models: support vector regression machine and random forest," *Procedia Structural Integrity*, vol. 17, pp. 698–703, 2019, doi:[10.1016/j.prostr.2019.08.093](https://doi.org/10.1016/j.prostr.2019.08.093).
59. Y. Freund and R. E. Schapire, "A decision-theoretic generalization of on-line learning and an application to boosting," *J Comput Syst Sci*, vol. 55, pp. 119–39, 1997, doi:[10.1006/jcss.1997.1504](https://doi.org/10.1006/jcss.1997.1504).
60. C.-H. Chien, T. Ajc, and C.-C. Wang, "Arima-adaboost hybrid approach for product quality prediction in advanced transformer manufacturing," *Advanced Engineering Informatics*, vol. 57, p. 102055, 2023, doi:[10.1016/j.aei.2023.102055](https://doi.org/10.1016/j.aei.2023.102055).
61. G. Varoquaux, L. Buitinck, G. Louppe, O. Grisel, F. Pedregosa, and A. Mueller, "Scikit-learn," *GetMobile: Mobile Computing and Communications*, vol. 19, pp. 29–33, 2015, doi:[10.1145/2786984.2786995](https://doi.org/10.1145/2786984.2786995).
62. Y. Hu, C. Gu, Z. Meng, and C. Shao, "Improve the model stability of dam's displacement prediction using a numerical-statistical combined model," *IEEE Access*, vol. 8, pp. 147 482–93, 2020, doi:[10.1109/ACCESS.2020.3014919](https://doi.org/10.1109/ACCESS.2020.3014919).
63. B. Wei, L. Chen, H. Li, D. Yuan, and G. Wang, "Optimized prediction model for concrete dam displacement based on signal residual amendment," *Appl Math Model*, vol. 78, pp. 20–36, 2020, doi:[10.1016/j.apm.2019.09.046](https://doi.org/10.1016/j.apm.2019.09.046).
64. S. Wang, C. Gu, and T. Bao, "Observed displacement data-based identification method of deformation time-varying effect of high concrete dams," *Sci China Technol Sci*, vol. 61, pp. 906–15, 2018, doi:[10.1007/s11431-016-9088-9](https://doi.org/10.1007/s11431-016-9088-9).
65. K. E. Taylor, "Summarizing multiple aspects of model performance in a single diagram," *Journal of Geophysical Research: Atmospheres*, vol. 106, pp. 7183–92, 2001, doi:[10.1029/2000JD900719](https://doi.org/10.1029/2000JD900719).
66. F. Kang, J. Li, and J. Dai, "Prediction of long-term temperature effect in structural health monitoring of concrete dams using support vector machines with jaya optimizer and salp swarm algorithms," *Advances in Engineering Software*, vol. 131, pp. 60–76, 2019, doi:[10.1016/j.advengsoft.2019.03.003](https://doi.org/10.1016/j.advengsoft.2019.03.003).
67. Q. Ren, M. Li, H. Li, and Y. Shen, "A novel deep learning prediction model for concrete dam displacements using interpretable mixed attention mechanism," *Advanced Engineering Informatics*, vol. 50, p. 101407, 2021, doi:[10.1016/j.aei.2021.101407](https://doi.org/10.1016/j.aei.2021.101407).